1098 *Chem. Mater.* **2004,** *16,* 1098−1103

Nanolaminates of Zirconia and Silica Using Atomic Layer Deposition

Lijuan Zhong,† Fang Chen,‡ Stephen A. Campbell,‡ and Wayne L. Gladfelter*,†

Departments of Chemistry and Electrical and Computer Engineering, University of Minnesota, Minneapolis, Minnesota 55455

Received September 10, 2003. Revised Manuscript Received January 14, 2004

In a low-pressure chemical vapor deposition reactor, alternating exposure of Si(100) substrates to tri(*tert*-butoxy) silanol and anhydrous zirconium nitrate deposited mixed films of zirconia and silica at 162 °C. The deposition rate, defined as the thickness (Å) per cycle, exhibited saturation behavior indicative of self-limiting growth. The maximum rate of approximately 12 Å/cycle exceeded the thickness expected for a single monolayer each of ZrO_2 and SiO_2. Metal composition of the films, as determined using Rutherford backscattering spectrometry, ranged from 3.3 to 49% zirconium. A singular reflection in the low-angle X-ray scattering pattern had a *d* spacing indicative of an ordered bilayer structure. The films were atomically smooth and their thickness was uniform across the entire substrate. Both the refractive indices, measured by ellipsometry, and the effective dielectric constants exhibited a linear dependence on the zirconium concentration.

Introduction

As the thickness of the gateoxide in field effect transistors approaches 2 nm, direct tunneling becomes problematic, making it necessary to replace the silicon dioxide layer with a material possessing a higher dielectric constant. The search for a suitable dielectric has covered many monometallic metal oxides (e.g., TiO_2, ZrO_2, HfO_2, Ta_2O_5, Al_2O_3, etc.) and several compound oxides such as $SrTiO_3$.[1−4] Recently, attention has focused on combinations of metal oxides that produce smoother amorphous films having fewer grain boundaries. Mixtures of ZrO_2 with a glass-forming oxide, such as SiO_2, is one system under investigation.[5−7]

Mixed ZrO_2/SiO_2 films have been deposited by sputtering,[7] plasma-enhanced CVD,[8] and atomic layer deposition (ALD).[9−12] ALD enables accurate control of film thickness and composition through self-limiting surface reactions.[13] The ALD of ZrO_2/SiO_2 has been accomplished by using individual silicon, zirconium, and oxygen source materials.[12] Recently, Ritala et al.[10] and Gordon et al.[9] described a two-precursor approach in which one of the precursors also acted as the oxygen source. Thus, ALD of ZrO_2/SiO_2 films was successful using $ZrCl_4$ and silicon alkoxides[10,11] or amido compounds of zirconium and hafnium used in conjunction with tri(*tert*-butoxy)silanol [(^{t}BuO)$_3$SiOH].[9] The presence of the hydroxy ligand in (^{t}BuO)$_3$SiOH, coupled with a facile isobutene elimination step, serve to enhance the SiO_2 deposition rate. In a study of the ALD of Al_2O_3/SiO_2 films, Gordon and co-workers discovered that as many as 30 monolayers of SiO_2 could be deposited during a single pulse of (^{t}BuO)$_3$SiOH.[14]

Anhydrous metal nitrates are carbon-, hydrogen-, and halogen-free single-source precursors that have been used in CVD[15,16] as well as ALD processes.[17] Solanki et al. recently reported the electrical properties of nonstoichiometric hafnium silicate films grown by $Hf(NO_3)_4$ and (^{t}BuO)$_3$SiOH.[18] In this article, we report the deposition of alternating layers of zirconia and silica and detail the film microstructure as a function of deposition conditions. X-ray scattering clearly demonstrates the layered, nanolaminate structure.

* To whom correspondence should be addressed. Phone: 612-624-4391. Fax: 612-626-8659. E-mail: gladfelt@chem.umn.edu.
† Department of Chemistry.
‡ Department of Electrical and Computer Engineering.

(1) Eisenbeiser, K.; Finder, J. M.; Yu, Z.; Ramdani, J.; Curless, J. A.; Hallmark, J. A.; Droopad, R.; Ooms, W. J.; Salem, L.; Bradshaw, S.; Overgaard, C. D. *Appl. Phys. Lett.* **2000**, *76*, 1324.
(2) McKee, R. A.; Walker, F. J.; Chisholm, M. F. *Phys. Rev. Lett.* **1998**, *81*, 3014.
(3) Yu, Z.; Ramdani, J.; Curless, J. A.; Overgaard, C. D.; Finder, J. M.; Droopad, R.; Eisenbeiser, K. W.; Hallmark, J. A.; Ooms, W. J.; Kaushik, V. S. *J. Vac. Sci. Technol. B* **2000**, *18*, 2139.
(4) Thomas, R.; Dube, D. C. *Ferroelectrics* **1999**, *225*, 905.
(5) Qi, W. J.; Nieh, R.; Dharmarajan, E.; Lee, B. H.; Jeon, Y.; Kang, L. G.; Onishi, K.; Lee, J. C. *Appl. Phys. Lett.* **2000**, *77*, 1704.
(6) Wilk, G. D.; Wallace, R. M.; Anthony, J. M. *J. Appl. Phys.* **2000**, *87*, 484.
(7) Wilk, G. D.; Wallace, R. M. *Appl. Phys. Lett.* **2000**, *76*, 112.
(8) Lucovsky, G.; Rayner, G. B. *Appl. Phys. Lett.* **2000**, *77*, 2912.
(9) Gordon, R. G.; Becker, J.; Hausmann, D.; Suh, S. *Chem. Mater.* **2001**, *13*, 2463.
(10) Ritala, M.; Kukli, K.; Rahtu, A.; Raisanen, P. I.; Leskelä, M.; Sajavaara, T.; Keinonen, J. *Science* **2000**, *288*, 319.
(11) Kim, W. K.; Kang, S. W.; Rhee, S. W.; Lee, N. I.; Lee, J. H.; Kang, H. K. *J. Vac. Sci. Technol., A* **2002**, *20*, 2096.
(12) Vainonen-Ahlgren, E.; Tois, E.; Ahlgren, T.; Khriachtchev, L.; Marles, J.; Haukka, S.; Tuominen, M. *Comput. Mater. Sci.* **2003**, *27*, 65.
(13) Suntola, T. *Mater. Sci. Rep.* **1989**, *4*, 261.
(14) Hausmann, D.; Becker, J.; Wang, S. L.; Gordon, R. G. *Science* **2002**, *298*, 402.
(15) Smith, R. C.; Hoilien, N.; Taylor, C. J.; Ma, T. Z.; Campbell, S. A.; Roberts, J. T.; Copel, M.; Buchanan, D. A.; Gribelyuk, M.; Gladfelter, W. L. *J. Electrochem. Soc.* **2000**, *147*, 3472.
(16) Colombo, D. G.; Gilmer, D. C.; Young, V. G., Jr.; Campbell, S. A.; Gladfelter, W. L. *Chem. Vap. Deposition* **1998**, *4*, 220.
(17) Conley, J. F.; Ono, Y.; Tweet, D. J.; Zhuang, W.; Solanki, R. *J. Appl. Phys.* **2003**, *93*, 712.
(18) He, W.; Solanki, R.; Conley, J. F.; Ono, Y. *J. Appl. Phys.* **2003**, *94*, 3657.

10.1021/cm0306111 CCC: $27.50 © 2004 American Chemical Society
Published on Web 02/21/2004

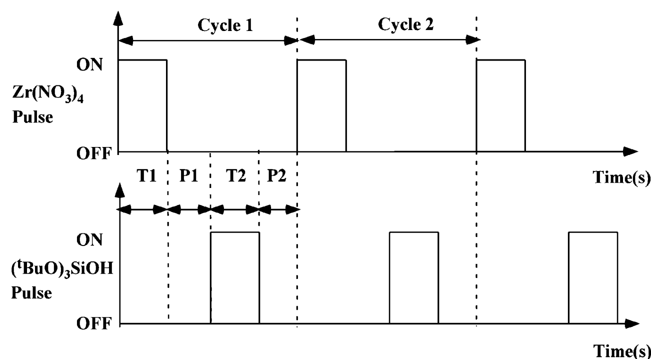

Figure 1. Pulse/purge sequence of the ALD process used to deposit ZrO_2/SiO_2 bilayers.

Experimental Section

Materials. Tri(*tert*-butoxy)silanol (99.9%) was purchased from Aldrich Company and used as received. Anhydrous zirconium nitrate [$Zr(NO_3)_4$] was synthesized via the reaction of $ZrCl_4$ and N_2O_5 using a modification of literature procedures[19,20] and then purified by sublimation at 95 °C. Both precursors were stored and transferred into precursor vessels under a dry N_2 atmosphere inside a glovebox. *Caution: Anhydrous metal nitrates are strong oxidants and care should be taken to avoid contact with organic compounds.*

Deposition Conditions. The films were grown on (100)-oriented *p*-Si single crystal substrates (approximately 1-in. square) in a cold-wall, low-pressure CVD reactor. The reactor chamber has been described in detail previously.[15] Substrates were degreased using methylene chloride, blown dry, and then placed into a solution consisting of 7 parts concentrated H_2SO_4 and 3 parts 30% H_2O_2. Immediately prior to deposition, a wafer was removed from the solution, rinsed thoroughly with deionized water, and dipped into a 10% hydrofluoric acid solution for 15 s. Substrates were then blown dry before being placed into the reactor, which was evacuated using a mechanical pump. High-purity N_2 was used as both carrier and purge gas. Gas lines were equipped with computer-controlled solenoid valves. After evacuation of the reactor, the N_2 purge gas flow into the chamber was started. The $Zr(NO_3)_4$ vessel was heated to 65 °C using Variac-controlled heating tape. The $(^tBuO)_3SiOH$ precursor vessel was warmed to 35 °C. All delivery lines were heated to approximately 75 °C to prevent condensation. The growth temperature of 162 ± 2 °C was chosen to avoid the self-decomposition of $Zr(NO_3)_4$ but high enough to induce complete reaction between $Zr(NO_3)_4$ and $(^tBuO)_3SiOH$. The molybdenum susceptor was heated to the growth temperature using a Variac-controlled 1000-W halogen lamp set within a parabolic, polished aluminum reflector. The susceptor temperature was measured by a thermocouple. Once the precursor vessels and susceptor reached their desired temperatures, the deposition sequence indicated in Figure 1 and the cycle count was started. The effect of $Zr(NO_3)_4$ and $(^tBuO)_3SiOH$ pulse time (T1 and T2, respectively) variation on thickness/cycle was determined experimentally. Purge times (P1 and P2) were typically set to exceed the precursor pulse times; however, these were not systematically studied. Deposition conditions are summarized in Table 1. Selected films underwent a postdeposition anneal for 30 s at 700 °C under N_2 in a rapid thermal annealer. The films were heated to 700 °C at a rate of 90 °C/s and remained at the elevated temperature for 30 s and then cooled within 7 min. These conditions were chosen to correspond to typical thermal treatments such dielectric films would encounter during subsequent microelectronic fabrication steps. One film was annealed at 1000 °C for 18 min in air in a tube furnace.

Thin Film Characterization. Rutherford backscattering spectrometry was performed using a spectrometer purchased from NEC and equipped with a MAS 1700 end station. The energy of the He^+ beam was 2.0 MeV and the beam current was 10 nA. The total charge collected was 10 μC. RBS spectra were modeled using HYPRA software to determine the atomic percentage of Zr, Si, and O present in the film. Carbon and nitrogen impurities were below the detection limit of RBS. No attempt was made to measure the hydrogen concentration in the films.

Table 1. Summary of Operating Conditionsfor the Deposition of Zirconia/Silica Films

parameter	condition
purge gas (N_2)	50−60 sccm
carrier gas (N_2)	25 sccm
deposition pressure	0.3−0.4 Torr
substrate temperature	162 °C
$Zr(NO_3)_4$ vessel temperature	65 °C
$(^tBuO)_3SiOH$ vessel temperature	35 °C
T1	2−20 s
P1	2−20 s
T2	1−24 s
P2	2−20 s

Ellipsometry at a 70° incident angle where $\lambda = 6328$ Å was used to measure the film thickness and refractive index simultaneously at three or more locations on each wafer, including the center, corner, and edge. The correct solution of thickness and refractive index was chosen by independently measuring the thickness on several films using cross-sectional SEM and RBS. Film crystallinity was evaluated using a Siemens D5005 X-ray diffractometer for as-deposited films and for films annealed at 700 °C under N_2 or at 1000 °C in air. Samples used for X-ray diffraction were typically 1000−1500 Å thick. Low-angle X-ray scattering measurements were carried out at the 2-BM bending magnet beamline of the Advanced Photon Source (APS) using a wavelength of 1.078 Å. Surface roughness was measured with an atomic force microscope (Digital Instruments Nanoscope III) operated in contact mode. The Si_3N_4 probe was scanned over a 2×2 μm area. The cross-sectional SEM backscattered electron image was collected on an Hitachi S-900 scanning electron microscope with an 8-keV accelerating voltage.

Electrical Characterization. With use of standard lithographic methods, capacitors were patterned on samples ranging in thickness from 300 to 500 Å. Platinum, deposited using a dc sputtering process, was used as the top electrode. Capacitance−voltage (C−V) properties were examined using an HP 4294A impedance analyzer, and current−voltage (*I*−*V*) measurements were acquired on an HP 4156A parameter analyzer. From graphs of the C−V data, the flat band voltage was estimated at the inflection point of the plot. To determine the dielectric constant, the capacitance was measured at a voltage that was shifted 1.1 V from the flat band voltage toward the region of charge accumulation. Further into the region of accumulation the C−V curves were flat. The effective dielectric constant, κ_{eff}, was calculated using the accumulation capacitance and the thickness obtained from ellipsometry (eq 1),

$$C = \kappa_{eff}\epsilon_0 A/t \qquad (1)$$

where ϵ_0 is the permittivity of free space, A is the area of the capacitor, and t is the film thickness.

Results

Film Deposition. At the relatively low temperature used in this study (162 °C) neither $Zr(NO_3)_4$ nor $(^tBuO)_3SiOH$ deposited films in the absence of the other. With use of the gas pulse sequence shown in Figure 1, mixed films of ZrO_2 and SiO_2 were formed. Figure 2 shows the variation of the growth rate (defined as the thickness/cycle) and Zr content (defined as [Zr at %/(Zr at % + Si at %)], according to RBS modeling results) as a function of the $Zr(NO_3)_4$ pulse time. The $(^tBuO)_3SiOH$

(19) Schmeisser, M. *Angew. Chem.* **1955**, *67*, 493.
(20) Field, B. O.; Hardy, C. J. *Proc. Chem. Soc.* **1962**, 76.

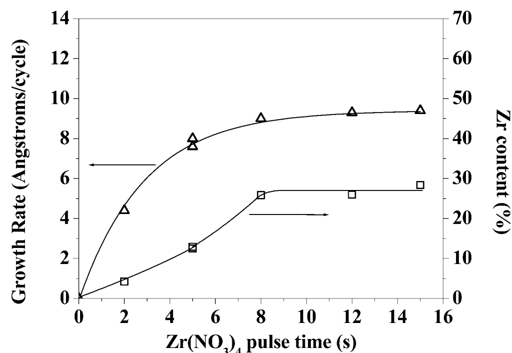

Figure 2. Growth rate (triangles) and Zr content (squares) as a function of the $Zr(NO_3)_4$ pulse time (T2: 5 s, P2: 10 s). P1 was 5, 10, and 15 s, respectively, when T1 was 2, 5, and ≥8 s.

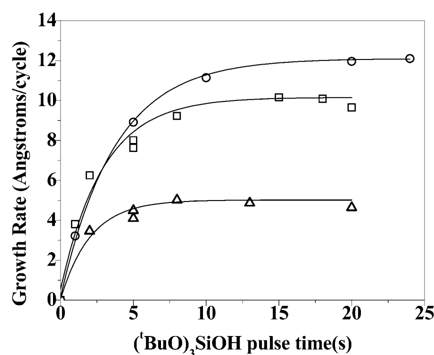

Figure 3. Growth rate as a function of the $(^tBuO)_3SiOH$ pulse time at three different $Zr(NO_3)_4$ exposure times: T1: 2 s, P1: 5s (triangles); T1: 5 s, P1: 10 s; (squares); T1: 8 s, P1: 15 s (circles). P2 was 2, 5, 10, 15, and 20 s, respectively, when T2 was 1, 2, 5, 8–20, and 24 s.

pulse and purge times were fixed at 5 and 10 s, respectively. Other deposition parameters, like precursor vessel temperatures and carrier and purge gas flow rates, were kept constant. As the $Zr(NO_3)_4$ pulse time increased, the growth rate saturated above 9 s. The Zr content reached a limiting value of 27%.

Figure 3 showsthe dependence of the growth rate on the $(^tBuO)_3SiOH$ pulse time. $Zr(NO_3)_4$ pulse time was fixed for each series at 2, 5, and 8 s, respectively, and all other deposition parameters were the same. As the $(^tBuO)_3SiOH$ pulse time increased, the growth rate saturated at 5, 10, and 12 Å/cycle, respectively, for the T1 values of 2, 5, and 8 s. No significant change in the growth rate was observed thereafter. Longer $(^tBuO)_3SiOH$ pulse times were needed to reach saturation as the $Zr(NO_3)_4$ pulse times increased. The Zr content indicated in Figure 4 decreased and reached limiting values of 3.4% (T1: 2 s), 11% (T1: 5 s), and 20% (T1: 8 s).

Figure 5 shows the linear behavior of film thickness as a function of the number of deposition cycles for two pulse sequences. Rutherford backscattering spectrometry was used to determine film composition as a function of depth. Even for those films with the largest repeating bilayer thickness created by the ALD process (∼12 Å), the depth resolution of RBS was insufficient to resolve the composition variations of the individual layers. All spectral modeling assumed a uniform elemental distribution throughout the film. Composition variation at the edge, corner, and center of three different wafers was examined and found to be ≤3%. The Zr contents ranged from 3.3 to 49%.

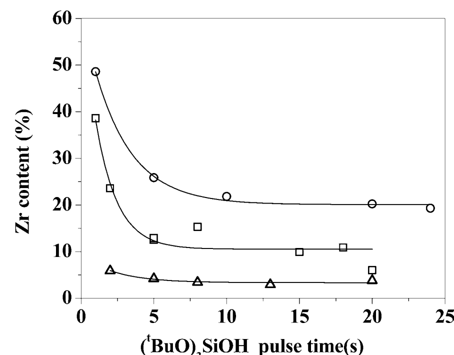

Figure 4. Film composition as a function of the $(^tBuO)_3SiOH$ pulse time at three different $Zr(NO_3)_4$ exposure times: T1: 2 s, P1: 5 s (triangles); T1: 5 s, P1: 10 s; (squares); T1: 8 s, P1: 15 s (circles). P2 was 2, 5, 10, 15, and 20 s, respectively, when T2 was 1, 2, 5, 8–20, and 24 s.

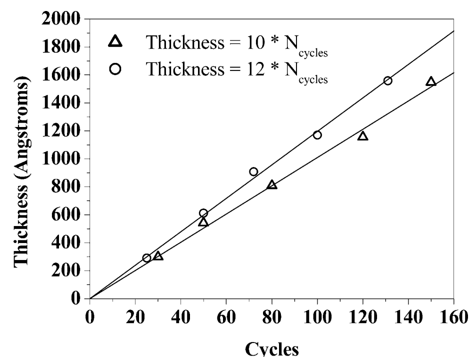

Figure 5. Film thickness (Å) measured by ellipsometry as a function of the number of cycles. T1: 8 s, P1: 12 s, T2: 20 s, P2: 15 s (circles), T1: 5 s, P1: 10 s, T2: 18 s, P2: 15 s (triangles).

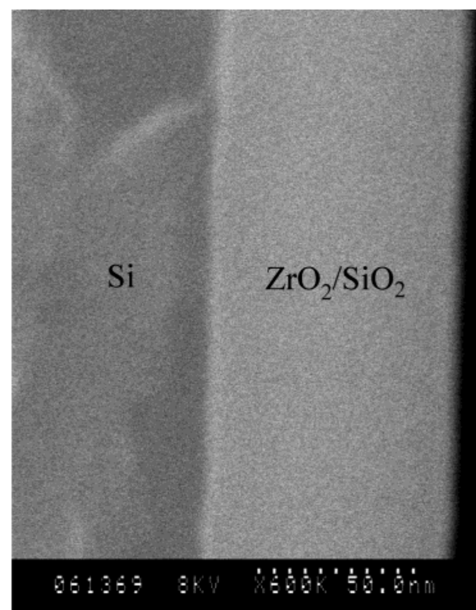

Figure 6. Cross-sectional scanning electron micrograph of a film deposited with 120 cycles of T1: 5 s, P1: 10 s, T2: 2 s, and P2: 5 s.

Film thickness (780 Å) of a sample grown with 120 cycles of T1: 5 s, P1: 10 s, T2: 2 s, and P2: 5 s was measured by cross-sectional SEM (Figure 6) and compared well to the ellipsometer results (750 Å). Figure 6 also established that the films were smooth. To quantify roughness, three films with different Zr content (10, 26,

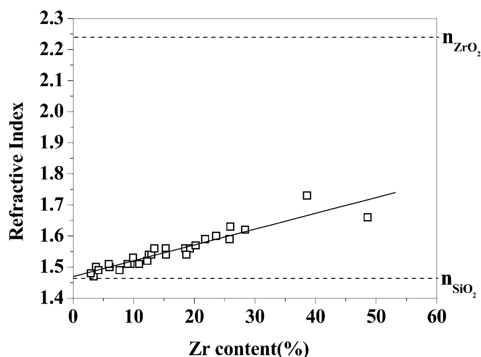

Figure 7. Refractive index as a function of composition.

Table 2. Summary of XRD Results

sample	T1 (s)	T2 (s)	d_{Cu}[a] (Å)	d_{APS}[b] (Å)	d_{ELP}[c] (Å)
A	2	5		na	4.1 (4.0)
B	5	1		na	3.9 (3.6)
C	5	5		na	7.6
D	5	15	~10	~10	10.1
E	5	18		na	10.3 (10.1)
F	5	20		na	9.7 (9.6)
G	8	20	12.3	12.1	12.6
H	8	20	11.4	11.4	11.7
I	8	20	11.7 (11.2)	na	11.9 (11.6)
J	12	5	9.1	8.8	9.3
K	15	5	9.1	8.9	9.4

[a] Calculated by $2d \sin \theta = \lambda$ for Cu Kα radiation ($\lambda = 1.54056$ Å); a dash indicates that no diffraction was observed. d is the bilayer thickness. The value in parentheses was determined after annealing the film for 30 s at 700 °C under N_2. [b] Calculated by $2d \sin \theta = \lambda$ ($\lambda = 1.078$ Å at APS); na indicates that no measurement was made. [c] Thickness per cycle calculated using the total thickness (measured using ellipsometry) divided by the number of cycles. The value in parentheses was determined after annealing the film for 30 s at 700 °C under N_2.

and 41%) were measured by AFM. The rms roughness ranged from 2.7 to 4.4 Å, which corresponded to 0.3–0.4% of the thickness of each film.

The refractive index measured at 6328 Å ranged from 1.4 to 1.8 and exhibited a linear relationship to film composition (Figure 7) as defined in eq 2.

$$\text{refractive index} = 1.470 + 0.0051^{*}\text{Zr}_{\text{content}} \quad (2)$$

The value of the y-intercept (1.47) corresponds to the known value (1.46) of the refractive index for amorphous SiO_2.[21] Extrapolation of the trend to 100% ZrO_2 predicts a value of 1.98. The refractive index of single-crystal ZrO_2 (monoclinic phase) is 2.24;[22] however, amorphous films of pure ZrO_2 typically have values ranging from 1.8 to 2.1.[23–26]

All of the as-deposited films were amorphous based on X-ray diffraction measurements on a Siemens D5005 X-ray diffractometer. A weak peak due to the ($\bar{1}11$) reflection of monoclinic ZrO_2 was observed in films with 41% Zr (entry B in Table 2). Of particular interest, however, was the appearance of a peak at low values of 2θ for films in which the $Zr(NO_3)_4$ exposure reached its saturation value (Table 2 and Figure 8). This reflection originates from the diffraction of X-rays from the periodic stack of ZrO_2–SiO_2 bilayers. The thickness of a bilayer was calculated using Bragg's law, and the resulting values were in agreement with the bilayer thickness calculated by dividing the total thickness (from ellipsometry) by the number of cycles used in the deposition (Table 2 and Figure 8).

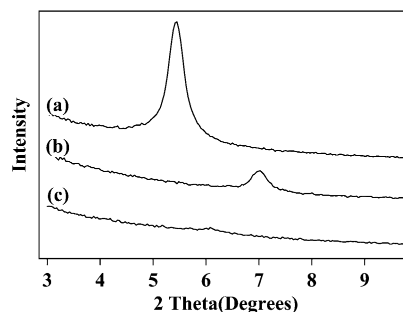

Figure 8. XRD of as-deposited films in a low-angle region using $\lambda = 1.078$ Å. The bilayer thickness values obtained by ellipsometry (d_{ELP}) and that derived from the XRD result (d_{APS}) and the Zr content for each film are as follows: (a) $d_{ELP} = 11.7$ Å, $d_{APS} = 11.4$ Å, Zr content = 20%; (b) $d_{ELP} = 9.3$ Å, $d_{APS} = 8.8$ Å, Zr content = 26%; (c) $d_{ELP} = 10.1$ Å, $d_{APS} \sim 10$ Å, Zr content = 10%.

Table 3. Dielectric Constant for Films with Varied Compositions

$Zr_{content}$ (%)	thickness (Å)	κ_{eff}	κ_{cal}[a]	$(\kappa_{eff} - \kappa_{cal})/\kappa_{cal}$ (%)
3.8	371	4.5	4.6	−2.2
4.2	204	3.8	4.6	−17.3
5.9	415	4.6	4.9	−6.1
7.7	298	4.2	5.2	−19.2
19	292	4.5	7.2	−37.5
39	455	10.2	10.7	−4.6
49	224	11.1	12.5	−11.2

[a] Calculated by the linear combination of κ_{ZrO2}(22) and κ_{SiO2}(3.9) weighted by their relative concentrations.

X-ray diffraction of selected films annealed at 700 °C for 30 s under nitrogen did not produce any detectable reflections from crystalline ZrO_2. The intensity of the low-angle peak for the film having Zr content of 20% (entry I) was attenuated and the d-spacing calculated (11.2 Å) shows a 4% contraction relative to the as-deposited film (11.7 Å). Contraction of 1–3% was also observed in the total thickness measured using ellipsometry. These results suggest the film densified at elevated temperature. Though only little change occurred relative to the as-deposited film after annealing at 700 °C for 30 s, more severe treatment (1000°C for 18 min in air) for the film with 41% Zr (entry D) resulted in a significant increase in the intensity of the ($\bar{1}11$) reflection of monoclinic ZrO_2. Despite the nearly one-to-one stoichiometry present in the as-deposited film, no diffraction peaks attributable to crystalline $ZrSiO_4$ were found.

Dielectric Constant. The values of the effective dielectric constant of the as-deposited films were calculated from the experimental capacitance measurements of the MIS structures in which p-doped silicon and platinum formed the bottom and top electrodes, respectively. As shown in Table 3, the dielectric constant increased in direct proportion to the concentration of Zr in the film. The value of the dielectric constant of

(21) Awazub, K.; Onuki, H. *J. Non-Cryst. Solids* **1997**, *215*, 176.
(22) Balzaretti, N. M.; Da Jornada, J. A. H. *Phys. Rev. B* **1995**, *52*, 9266.
(23) Yu, J. J.; Boyd, I. W. *Appl. Surf. Sci.* **2003**, *208–209*, 374.
(24) Nam, S. W.; Yoo, J. H.; Kim, H. Y.; Kang, S. K.; Ko, D. H.; Yang, C. W. *J. Vac. Sci. Technol., A* **2001**, *19*, 1720.
(25) Levichkova, M.; Mankov, V.; Starbov, N.; Karashanova, D.; Mednikarov, B. *Surf. Coat. Technol.* **2001**, *141*, 70.
(26) Venkataraj, S.; Jayavel, R.; Wuttiga, M. *J. Appl. Phys.* **2002**, *92*, 3599.

the bilayer structure can be calculated according to eq 1. Neglecting the impact of changes in the molar volume of the mixed oxides,[27] Table 3 compares the experimental dielectric constant (κ_{eff}) to that calculated based on a linear combination of a κ_{ZrO2} of 22 and a κ_{SiO2} of 3.9 weighted by their relative concentrations.

Discussion

Film Microstructure. During each of the depositions, the substrate was maintained at 162 °C and exposed alternatively to separate flows of $Zr(NO_3)_4$ and $(^tBuO)_3SiOH$. This temperature was chosen because neither of the individual precursors alone deposits measurable films at 162 °C. After deposition, the film thickness was measured by ellipsometry. For several films the thickness values were also extracted from RBS and cross-sectional SEM measurements; both results correlated well with the ellipsometric data. For both precursors, the deposition rates, defined as Å/cycle, displayed saturation behavior typical of atomic layer depositions.

We focus first on the microstructure of the films grown under saturation conditions for both precursors. In an ALD process in which one layer each of ZrO_2 and SiO_2 would be deposited per cycle, the maximum film thickness would be approximately 4.4 Å. This estimate is based on the monoclinic phase of zirconia, in which a layer of ZrO_2 in the $a-b$ plane has a thickness of 1/2 c or 2.6 Å. Because the films were amorphous, the choice of this plane was arbitrary, especially considering that similar values were obtained along the a or b axes. The value of 1.8 Å for SiO_2 monolayer thickness was based on 1/3 c in α-quartz. As shown in Table 2, entries G, H, and I were deposited under saturation conditions and produced films with a thickness of 12 Å, nearly 3 times the value of a ZrO_2/SiO_2 bilayer structure. The Zr concentration in film I was 20% consistent with deposition of 4 SiO_2 units for each ZrO_2. With use of the above dimensions for the SiO_2 and ZrO_2 monolayers, the stoichiometry found in film I should give a thickness/cycle of 9.8 Å. That the experimental value was somewhat higher for the amorphous films (as determined by XRD) was not unreasonable. In a recent study of the CVD of ZrO_2, film densities were found to range from 65 to 88% of the single-crystal value.[28]

For films grown under saturation conditions X-ray diffraction measurements revealed the appearance of a superlattice spacing that was very close to that calculated for the bilayer thickness (Table 2 and Figure 8). Such a diffraction peak would require a periodic oscillation of the electron density within each film. This excludes a microstructure in which the ZrO_2 and SiO_2 units are uniformly distributed throughout the bilayer and is consistent with the nanolaminate structure shown in Scheme 1. In this scheme, formation of a complete monolayer of ZrO_2 would occur during each $Zr(NO_3)_4$ pulse. In Table 2 and Figure 8, films that did not reach the saturation coverage of ZrO_2 (<8 s $Zr(NO_3)_4$ pulse times) did not display this low-angle reflection. Presumably, the gaps in the ZrO_2 film would degrade

Scheme 1. Three Bilayers Showing the Proposed Nanolaminate Structure[a]

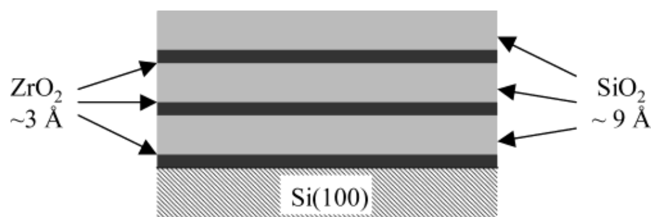

[a] The dimensions are films in which both precursors reached saturation exposure.

electron density contrast and perhaps increase roughness. Both factors would decrease the intensity of a bilayer reflection. Decreasing the exposure time of $(^tBuO)_3SiOH$ below the saturation value, however, did not cause the low-angle reflection to disappear. Rather, the d spacing decreased in accordance with the value calculated from ellipsometry. We conclude that the SiO_2 layer thickness is decreased, while the ZrO_2 layer is unchanged. Consistent with this picture, the Zr concentration in these films increases.

Chemistry of the Deposition. On the basis of the molecular structures of the two precursors, formation of Zr−O−Si linkages with corresponding elimination of HNO_3 would be expected. Equation 3 is related to the known synthesis of $Zr[OSi(O^tBu)_3]_4$ from $Zr(NEt_2)_4$ and $(^tBuO)_3SiOH$.[29]

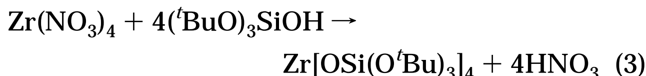

$$Zr(NO_3)_4 + 4(^tBuO)_3SiOH \rightarrow Zr[OSi(O^tBu)_3]_4 + 4HNO_3 \quad (3)$$

Considering the relationship this reaction bears to well-established ALD processes such as the deposition of ZrO_2 from $ZrCl_4$ and H_2O[30−32] (i.e., labile ligands on zirconium and a reactive OH group), Scheme 2 represents a reasonable sequence of reactions for forming the nanolaminate films. After completion of the $(^tBuO)_3SiOH$ addition, cleavage of the O−C bonds of the *tert*-butoxy groups and condensation of the SiOH groups must occur. Tilley and co-workers have extensively studied the chemistry of metal complexes bearing the tri(*tert*-butoxy)siloxy ligand and their conversion into solid state mixed-metal oxides.[29,33] Of special relevance to the work described in this paper is the characterization of $Zr[OSi(O^tBu)_3]_4$. Upon thermolysis at temperatures as low as 137 °C, this compound eliminates isobutene and water to form amorphous $ZrO_2 \cdot 4SiO_2$ (eq 4).

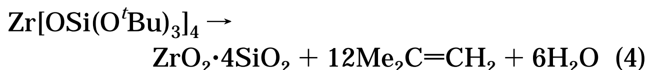

$$Zr[OSi(O^tBu)_3]_4 \rightarrow ZrO_2 \cdot 4SiO_2 + 12Me_2C{=}CH_2 + 6H_2O \quad (4)$$

As suggested in Scheme 2, this chemistry could complete the ALD process and regenerate a SiOH group needed to begin the next cycle.

(27) Kurtz, H. A.; Devine, R. A. B. *Appl. Phys. Lett.* **2001**, *79*, 2342.
(28) Burleson, D. J.; Roberts, J. T.; Gladfelter, W. L.; Campbell, S. A.; Smith, R. C. *Chem. Mater.* **2002**, *14*, 1269.
(29) Terry, K. W.; Lugmair, C. G.; Tilley, T. D. *J. Am. Chem. Soc.* **1997**, *119*, 9745.
(30) Gopel, M.; Gribelyuk, M.; Gusev, E. *Appl. Phys. Lett.* **2000**, *76*, 436.
(31) Ritala, M.; Leskelä, M. *Appl. Surf. Sci.* **1994**, *75*, 333.
(32) Kukli, K.; Ihanus, J.; Ritala, M.; Leskelä, M. *J. Electrochem. Soc.* **1997**, *144*, 300.
(33) Kriesel, J. W.; Sander, M. S.; Tilley, T. D. *Adv. Mater.* **2001**, *13*, 331.

Scheme 2. Possible Reaction Sequence for Forming the Zirconia/Silica Films

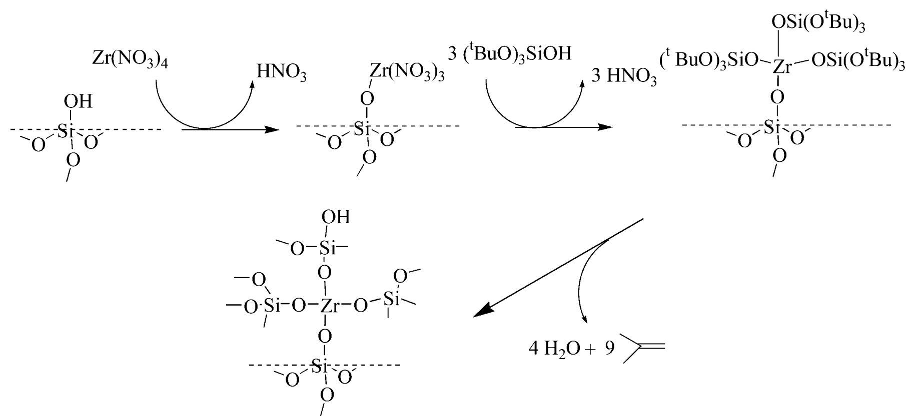

The specific stoichiometry of the final film would depend on the number of (^{t}BuO)$_3$SiOH ligands substituting on each zirconium. Considering that at least one Zr valence site will be occupied by the Si−O−Zr connection to the previous layer, up to three (^{t}BuO)$_3$SiOH ligands could be added. Equations 5−7 describe the idealized stoichiometries. Films of noninteger ratios of Zr/Si could be formed by mixing two or more equations.

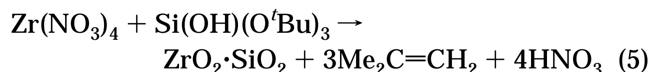

$$Zr(NO_3)_4 + Si(OH)(O^tBu)_3 \rightarrow ZrO_2{\cdot}SiO_2 + 3Me_2C{=}CH_2 + 4HNO_3 \quad (5)$$

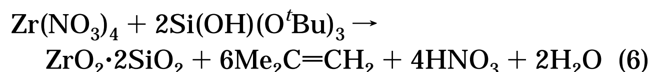

$$Zr(NO_3)_4 + 2Si(OH)(O^tBu)_3 \rightarrow ZrO_2{\cdot}2SiO_2 + 6Me_2C{=}CH_2 + 4HNO_3 + 2H_2O \quad (6)$$

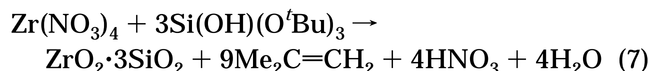

$$Zr(NO_3)_4 + 3Si(OH)(O^tBu)_3 \rightarrow ZrO_2{\cdot}3SiO_2 + 9Me_2C{=}CH_2 + 4HNO_3 + 4H_2O \quad (7)$$

The highest zirconium content achieved in this study was 49%, consistent with the limit represented by eq 5. These reactions alone, however, cannot explain the zirconium concentrations below 25% found in many of the films including those grown under conditions in which both precursors achieved surface saturation. Gordon and co-workers established the effectiveness of (^{t}BuO)$_3$SiOH as a SiO_2 source in the ALD of $ZrO_2{\cdot}nSiO_2$, $HfO_2{\cdot}nSiO_2$, and $Al_2O_3{\cdot}nSiO_2$ films in conjunction with $Zr(NEt_2)_4$, $Hf(NEt_2)_4$, and Al_2Me_6,[9,14] respectively. In all cases, the film thickness per cycle was large relative to results reported in other ALD processes. In the alumina case, the film thickness per cycle was consistent with the addition of as many as 30 monolayers of SiO_2 per Al_2O_3 monolayer.[14] To explain this behavior, a novel insertion reaction (eq 8) was proposed and supported by computational studies, suggesting the existence of a low-energy mechanistic pathway.

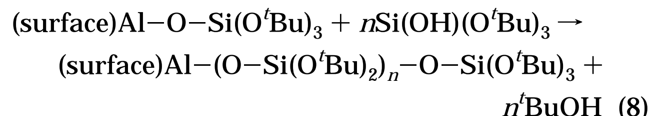

$$\text{(surface)Al}{-}O{-}Si(O^tBu)_3 + n\,Si(OH)(O^tBu)_3 \rightarrow \text{(surface)Al}{-}(O{-}Si(O^tBu)_2)_n{-}O{-}Si(O^tBu)_3 + n\,^tBuOH \quad (8)$$

In the current study we observed films with as little as 3% Zr, which would correspond to 28 equiv of SiO_2/equiv of ZrO_2.

An alternative to the Gordon reaction (eq 8) for decreasing the ZrO_2/SiO_2 ratio could involve catalytic dehydration of (^{t}BuO)$_3$SiOH. In Tilley and co-workers' study of Zr[OSi(O^{t}Bu)$_3$]$_4$, they noted that "the gel formed from hydrolysis of **1** [Zr[OSi(O^{t}Bu)$_3$]$_4$] efficiently catalyzes the dehydration of ^{t}BuOH and (^{t}BuO)$_3$SiOH to isobutene".[29] Dehydration of (^{t}BuO)$_3$SiOH would also produce SiO_2 and, thus, decrease the ZrO_2/SiO_2 ratio of the gel remaining in the mixture. There are important differences between reactions conducted on dense surfaces under vacuum vs on high surface area gels in solution. More research is needed to establish the details of this important reaction.

Conclusions

Alternating exposure of silicon substrates at 162 °C to anhydrous zirconium nitrate and tri(*tert*-butoxy)-silanol produce smooth, amorphous films. Both the thickness deposited per exposure cycle and the ratio of ZrO_2 to SiO_2 requires a process involving multiple SiO_2 units added per each ZrO_2. Films deposited under conditions leading to the saturation of ZrO_2 per layer displayed an ordered structure within each bilayer. Both the refractive index and dielectric constant displayed a linear correlation to composition: a feature that may be of value in device design and construction.

Acknowledgment. This research was supported by funds from the National Science Foundation [CHE-0076141] and the Semiconductor Research Corporation. Use of the Advanced Photon Source was supported by the U.S. Department of Energy, Office of Science, Office of Basic Energy Sciences, under Contract No. W-31-109-Eng-3. We are grateful to Dr. Yong Chu for assistance in the measurement of low-angle XRD patterns at APS and to Professor Solanki for a preprint of their study prior to publication.

CM0306111